Published in final edited form as:
Chemistry. 2012 July 27; 18(31): 9669–9676. doi:10.1002/chem.201200266.

Synthesis and Characterization of a Hypoxia-Sensitive MRI Probe

Federico A. Rojas-Quijano[a], **Gyula Tircsó**[b], **Enikő Tircsóné Benyó**[b], **Zsolt Baranyai**[b], **Huan Tran Hoang**[b], **Ferenc K. Kálmán**[b], **Praveen K. Gulaka**[c], **Vikram D. Kodibagkar**[c], **Silvio Aime**[d], **Zoltán Kovács**[a], and **A. Dean Sherry**[a,e]

Gyula Tircsó: gyula.tircso@science.unideb.hu; A. Dean Sherry: dean.sherry@utsouthwestern.edu

[a]Advanced Imaging Research Center, University of Texas Southwestern Medical Center, 5323 Harry Hines Boulevard, Dallas, Texas 75390 (USA), Fax: (+1) 214-645-2744

[b]Department of Inorganic and Analytical Chemistry, University of Debrecen, Egyetem tér 1, Debrecen, H-4010 (Hungary), Fax: (+36) 52-518-660

[c]Department of Radiology, University of Texas Southwestern Medical Center, 5323 Harry Hines Boulevard, Dallas, Texas 75390 (USA)

[d]Department of Chemistry IFM & Molecular Imaging Center, Università degli Studi di Torino, Via P. Giuria 7, 10125 Torino (Italy)

[e]Chemistry Department, University of Texas at Dallas, 5323 Harry Hines Boulevard, Dallas, Texas 75390 (USA), Fax: (+1) 972-883-2925

Abstract

Tissue hypoxia occurs in pathologic conditions such as cancer, ischemic heart disease and stroke when oxygen demand is greater than oxygen supply. An imaging method that can differentiate hypoxic *versus* normoxic tissue could have an immediate impact on therapy choices. In this work, the gadolinium complex of 1,4,7,10-tetraaza-1,4,7,10-tetraacetate (DOTA) having a 2-nitroimidazole attached to one carboxyl group *via* an amide linkage was prepared, characterized and tested as a hypoxia-sensitive MRI agent. A control complex, Gd(DO3A-monobutylamide), was also prepared in order to test whether the nitroimidazole side-chain alters either the water proton T_1 relaxivity or the thermodynamic stability of the complex. The stabilities of these complexes were lower than that of $Gd(DOTA)^-$ as expected for mono-amide derivatives. The water proton T_1 relaxivity (r_1), bound water residence lifetime (τ_M) and rotational correlation time (τ_R) of both complexes was determined by relaxivity measurements, variable temperature ^{17}O NMR and proton nuclear magnetic relaxation dispersion (NMRD) studies. The resulting parameters ($r_1 = 6.38\ m_M^{-1}s^{-1}$ at 20 MHz, $\tau_M = 0.71$ μs, $\tau_R = 141$ ps) determined for the nitroimidazole derivative closely parallel those of other Gd(DO3A-monoamide) complexes of similar molecular size. *In vitro* MR imaging experiments using 9L rat glioma cells maintained under nitrogen (hypoxic) *versus* oxygen (normoxic) gas showed that both agents enter cells but only the nitroimidazole derivative is trapped in cells maintained under N_2 as evidenced by ~2-fold decrease in T_1 measured for hypoxic cells *versus* normoxic cells exposed to this agent. These results suggest that the nitroimidazole derivative may serve as a molecular reporter for discriminating hypoxic *versus* normoxic tissues by MRI.

Correspondence to: Gyula Tircsó, gyula.tircso@science.unideb.hu; A. Dean Sherry, dean.sherry@utsouthwestern.edusherry@utdallas.edu.

Supporting information for this article is available on the WWW under http://www.chemeurj.org/ or from the author.

Keywords

imaging agents; ligand design; stability; relaxation properties; imaging of hypoxic tissue

Introduction

Tissue hypoxia usually reflects a locally restricted oxygen supply (ischemia) and/or an abnormal increase in oxygen consumption. In clinical practice, hypoxia is related to a variety of pathologic conditions including cancer, ischemic heart disease and stroke. Locally advanced solid tumors often have hypoxic or anoxic regions distributed heterogeneously throughout the tumor as a result from a structurally or functionally abnormal vasculature. Tumor hypoxia is commonly associated with a poor prognosis after radiation and chemotherapy and hypoxia can influence many aspects of tumor proliferation such as growth, apoptosis, angiogenesis and metastasis.[1,2]

In 1955, 2-nitroimidazole was shown to be active against certain anaerobic bacterial infections.[3] Later it was discovered that 2-nitroimidazole analogs could be used to sensitize hypoxic tumors to ionizing radiation.[4,5] Further research on the mechanism of action of this compound revealed that it was capable of accumulating in hypoxic tissue due to selective enzyme-mediated reduction of the nitro group under low oxygen conditions.[6] The diverse bioactivity of nitroimidazoles and related nitroaromatic compounds has the same underlying mechanism; the activities of these compounds depend on the redox potential of the nitro group.[7] The first step of this intracellular process involves the one-electron reduction of the nitro group to a radical anion, which undergoes further reduction in hypoxic cells but is rapidly oxidized back to the nitro compound under normoxic conditions. The reduction potential of the nitro group in nitroimidazoles is sensitive to its position in the imidazole ring and this correlates with hypoxia sensitivity.[8] Given the prospect of nitroimidazole as a platform for hypoxia-homing probes, several radiolabeled nitroimidazole derivatives and related compounds have been tested as imaging probes of hypoxic tissue *in vivo*.[9] Most prominent among theses have been the ^{18}F labeled fluoromisonidazole (^{18}F-FMISO)[10] for PET imaging and the ^{99m}Tc labeled propylene amineoxime (BMS181321)[11] for SPECT imaging. Cyclen (1,4,7,10-tetraazacyclododecane)-based nitroimidazole derivatives tagged with $^{67}Ga^{III}$, $^{153}Gd^{III}$ or $^{177}Lu^{III}$ have shown only moderate tumor localization.[12–14] Although several multi-fluorinated derivatives of 2-nitroimidazole have been synthesized and used to assess tumor hypoxia by ^{19}F NMR, Gd^{III}-based nitroimidazole derivatives for ^{1}H MRI have not been reported.[15–17] While MRI is considerably less sensitive than nuclear medicine for molecular imaging, it does offer the advantage of wide clinical availability, lack of radiation and high resolution anatomical images. For these reasons, we initiated a program to develop gadolinium-based 2-nitroimidazole derivatives and to evaluate the potential of such agents for detecting hypoxic cells by MRI.

Results and Discussion

Ligand design and synthesis

DOTA (1,4,7,10-tetraaza cyclododecane-1,4,7,10-tetraacetic acid) was selected as the chelate for the conjugation to 2-nitroimidazole because Gd^{III} complexes with DOTA-like ligands have high thermodynamic stability, are kinetically inert and have favorable relaxation properties.[18,19] The 2-nitroimidazole vector was selected based on its one-electron reduction potential, known to fall in the range of −330 to −450 mV, which allows for its entrapment and exclusive reduction under hypoxic conditions as it has been previously reported in the literature by many scientists (vide supra). Since conjugation of

DOTA to a targeting vector via a single carboxyl group is relatively straightforward,[20] a 2-nitroimidazole moiety with an extended side-chain containing a primary amino group was chosen for conjugation (Scheme 1). This design affords a neutral Gd^{III} complex which would hopefully help facilitate cellular uptake. It was anticipated that the relatively long linkage between Gd(DO3A-monoamide) unit and the nitroimidazole moiety in **3** would minimize any unwanted interference between the Gd^{III} coordination sphere and the nitroimidazole unit and, at the same time, increase complex lipophilicity. In addition, the linker does not contain groups that can engage in prototropic equilibria at physiological pH and should therefore not affect the redox potential of the nitroimidazole unit.[8,21] The synthesis of the target ligand is outlined in Scheme 1.

The protected DO3A-monoamide derivative **1** was obtained by alkylating DO3A-tris(*tert*-butyl ester) with methyl chloroacetate and reacting the resulting methyl ester with excess diaminobutane (putrescine) following a slight modification of a published procedure (ESI).[22] Nitroimidazoyl hexanoic acid (**2**) was synthesized by alkylation of 2-nitroimidazole with ethyl bromohexanoate followed by the cleavage of the ethyl group in concentrated HCl as previously reported.[23] The imidazoyl acid **2** and macrocyclic amine **1** where then coupled using standard HBTU/HOBt chemistry.[24,25] The *tert*-butyl protecting groups of the intermediate ester were cleaved using trifluoroacetic acid (TFA) and the crude product was purified by HPLC to give pure **3** (28% yield). Gd(**3**) was obtained in quantitative yield by reaction of **3** with $GdCl_3$ at pH 6.

Ligand protonation and complex stability constants

The coordination environment (four macrocyclic N donor atoms, three carboxylate O donor atoms and one amide O donor atom) provided by ligand **3** is typical of a DOTA- and DO3A-bioconjugate in which the chelator is attached to the biomolecule through one of the acetate pendant arms of the ligand.[20] Despite the widespread use of these ligands to chelate Gd^{3+} for MRI and various radioactive lanthanide ions for radiopharmaceutical applications, only a limited number of papers have appeared on the thermodynamic stability, formation and dissociation kinetics of DO3A-monoamides.[26,27] Here, we report the thermodynamic stabilities of the Ce(**3**), Gd(**3**) and Yb(**3**) and the results of ^{1}H and ^{17}O-NMR relaxometric studies of Gd(**3**). The results are also compared to corresponding data for Ce(**6**), Gd(**6**) and Yb(**6**).

pH-potentiometry is considered the gold standard technique for determining the protonation constants of polyaminopolycarboxylate ligands and thermodynamic stability constants of complexes formed with various metal ions. The protonation constants obtained from fitting the pH-potentiometric data for ligands **3** and **6** are presented in Table 1 along with the literature data for DOTA (**4**) and two amide derivatives, DO3A-monopropylamide (**5**) and DOTA-tetramethylamide (**7**). The trends found for the protonation constants of these ligands are similar, except for DOTA- tetra- methylamide (**7**) (Chart 1). For DOTA and DO3A-monoamide derivatives (**3** and **6**), the first two protonation constants (which have been traced to protonation at ring nitrogen atoms positioned *trans*- to one another) are relatively high, while the remaining log K_i^H values (reflecting protonation of the carboxylates) are much lower. For the monoamide ligands studied here, **3** and **6**, five protonation steps were observed in the pH range of 2–12. The total basicity of these ligands (expressed as the sum of the protonation constants, log β_4) is lower than that of DOTA, reflecting the lower basicity of the macrocyclic N-atoms.[28,29] The protonation constants of **6** as determined previously by pH-potentiometry in 0.1 M Me_4NCl (log β_4 = 27.94) were found to be somewhat higher than the values measured here in 1.0 M KCl (log β_4 = 26.54).[30] This can be attributed to the formation of a weak potassium complex in the presence of 1.0 M K^I ions (a similar decrease in basicity was observed for DOTA when the protonation constants were

measured in the presence of KCl *versus* Me_4NCl).[31] Interestingly, the first protonation constant of **3** is slightly lower (0.4 log *K* units) than that of **6**, presumably reflecting the elongated side arm on the amide. A similar decrease in the basicity was also observed for some alkyl-EDTA derivatives where an increase in the length of the alkyl substituent had a noticeable effect on the first protonation constant (see Table S1, ESI).

The formation equilibria between these macrocyclic ligands and the Ln^{III} ions cannot be studied by direct pH-potentiometric titration because of slow formation kinetics. Hence, the stability constants were determined by use of the "out-of-cell" technique using separate samples for each titration point (total of 16 points). The stability constants of some Ln(**3**) and Ln(**6**) complexes, assuming formation of only 1:1 complexes, are listed in Table 2. The standard deviations associated with these constants significantly decreased when the formation of monoprotonated species (LnLH) was also taken into consideration in the calculations. This suggests that protonation of the complexes also occurs under these conditions. The Ce(**6**) system was an exception, as the inclusion of the protonated species in the equilibrium model for this complex resulted in a significant increase in the standard deviation of fitted parameters.

As expected, the stabilities of all Ln^{III} complexes increase with decreasing lanthanide ion size, $Ce^{III} < Gd^{III} < Lu^{III}$ (Table 2).[37] The stabilities of all Ln(**3**) complexes were similar to the corresponding Ln(**6**) complexes, as expected for similar DO3A-monoamide structures. This indicates that incorporation of the elongated nitroimidazole-containing pendant arm does little to alter complex stability. However, these complexes are about four orders of magnitude less stable than the corresponding $Ln(DOTA)^-$ complexes due to the substitution of a carboxylate in DOTA for the weaker amide donor atom in **3** and **6.** This is also reflected in the total basicity of **3** and **6** compared to DOTA. Further substitution of acetate arms for amides results in even lower stabilities as illustrated by the stability of the Ln^{III} complexes of **7**. It is worth noting that the stability constant values measured in the presence of KCl represent a lower limit since these calculations assume no significant interaction between the ligands and K^I ions, likely an invalid assumption. These results indicate that DO3A-monobutylamide (**6**) serves as a good model for the nitroimidazole ligand, **3**, and other similar DOTA- or DO3A-bioconjugate systems.

Relaxometric studies

MRI contrast agents are typically characterized by a T_1 proton relaxivity (r_{1p}) value. The relaxivity (r_{1p}) of low molecular weight GdL that has rapid water exchange kinetics is dominated by the inner-sphere contribution (r_{1p}^{is}). The Solomon-Bloembergen-Morgan (SBM) theory of relaxivity predicts that r_{1p}^{is} is dependent on several parameters including the number of inner sphere water molecules (q), the longitudinal relaxation time of the protons of the water molecule(s) in the inner coordination sphere (T_{1M}^H), the residence time of the inner-sphere water molecule(s) (τ_M) and the tumbling rate of the paramagnetic complex in solution (τ_R, rotational correlation time).[38] At clinically relevant fields (1.5 – 3 T), the relaxivity is largely determined by τ_M and τ_R. These constants can be obtained by fitting of variable temperature ^{17}O NMR (τ_M) and ^1H nuclear magnetic relaxation dispersion (NMRD) data (τ_R).[38–40] At 20 MHz, 25°C and pH=7, the relaxivity (r_{1p}) of Gd(**3**) and Gd(**6**) were 6.38 ± 0.04 $m_M^{-1}s^{-1}$ and 5.05 ± 0.02 $m_M^{-1}s^{-1}$, respectively, measured at 20 MHz. The r_{1p} value of Gd(**3**) is about 30% higher than that of Gd(**6**), reflecting its higher molecular weight (larger size) and consequently longer rotational correlation time (τ_R). The relaxivity of Gd(**6**) is nearly the same as that of Gd(**8**) (r_{1p} = 5.0 $m_M^{-1}s^{-1}$, 25°C, 20 MHz), a Gd-complex of similar molecular weight and size.[41]

Temperature dependence of relaxivity—The relaxivities of Gd(**3**) and Gd(**6**) were also measured at 37°C (20 MHz) and found to be only slightly lower (5.25 ± 0.05 and 4.12 ± 0.02 $m_M^{-1}s^{-1}$, respectively) than the values measured at 25°C. The relaxivity of $Gd(DOTA)^-$ has a similar temperature dependence at this field, decreasing from 4.7 $m_M^{-1}s^{-1}$ to 3.6 $m_M^{-1}s^{-1}$ as the temperature is increased from 25 to 37°C. This behavior is expected for fast inner-sphere water exchange systems. It has been shown that the relaxivity of low molecular weight Gd-polyaminopolycarboxylate complexes whose bound water lifetime falls into the fast exchange regime ($T_{1M} >> \tau_M$) decreases exponentially with increasing temperature due to a decrease of the contribution of both r_{1p}^{is} (the residence time of the bound water molecule decreases) and r_{1p}^{os} (the diffusion rate of the water molecules increases on the surface of the complex). This has been observed for the Gd^{III} complexes of DOTA-like ligands that have two inner sphere water molecules (q = 2) (DO3A, PCTA) and consequently fast water exchange rates.[27,41,42] However, as the bound water lifetime approaches the slow exchange condition ($T_{1M} \approx \tau_M$), the relaxivity becomes exchange limited and its temperature dependence is less pronounced.[43,44]

Variable temperature ^{17}O NMR—The water exchange dynamics in Gd(**3**) and Gd(**6**) were studied by variable temperature ^{17}O NMR measurements. The temperature dependent profiles of the water ^{17}O NMR transverse relaxation rates for Gd(**3**) and Gd(**6**) (Figure 1) are similar to those reported previously for Gd^{III} complexes of other small molecular weight complexes such as Gd(**7**).[41] The maximum in the R_{2p} *versus* temperature curves for Gd(**3**) and Gd(**6**) were observed at about the same temperature as that reported previously for Gd(**8**) while the maximum observed for $Gd(DOTA)^-$ is shifted to lower temperatures, reflecting faster water exchange.[41,42] The residence time (τ_M) of the inner-sphere water molecule was determined by fitting these data to Swift-Connick theory.[45,44] The value found here for Gd(**3**) (0.71 μs) (Table 3) is about 50% of the value found for Gd(**8**) (1.3 μs) and about four times longer than the value found for $Gd(DOTA)^-$ (τ_M = 0.23 μs at 298 K).[38,41] These values are consistent with the empirical observation that substitution of one carboxylate for an amide results in an approximately 3- to 4-fold decrease in the metal bound water exchange rate in Ln-complexes of polyaminopolycarboxylate type ligands.[46] The relatively long water residence times suggest that the water exchange in these complexes likely occur *via* a dissociative mechanism.[46]

Magnetic field dependence—The magnetic field dependence of the proton relaxation rates (NMRD profiles) was also measured for Gd(**3**) and Gd(**6**) at 25°C and pH 7 (Figure 1). Among other relaxation parameters, the rotational correlation time (τ_R) can be determined from the magnetic field dependence of the longitudinal relaxation rate of the complex.

In a typical NMRD experiment, a field-cycling relaxometer is used to measure the longitudinal relaxation rates of the solvent protons in the presence of the paramagnetic complex over a continuum of magnetic fields that range from 0.01 MHz up to ~70 MHz. Normally, τ_M is independently determined by variable temperature ^{17}O NMR, while the inner-sphere relaxivity parameters are obtained by fitting the NMRD profiles to the Solomon–Bloembergen–Morgan equations and the outer-sphere parameters are determined by fitting the data to Freed's equations.[47,48] The solid curves through the experimental data points (Figure 1) represent the best fit calculated values obtained by use of the relaxation parameters summarized in Table 3. The NMRD profile of both complexes show a single dispersion centered near 4 MHz with two plateaus in the low and high magnetic field regions. (The rotational correlation times of the complexes Gd(**6**) (τ_R = 86 ps) and Gd(**8**) (τ_R =70 ps) are similar, whereas the τ_R value of the complex Gd(**3**) (141 ps) is about twice as high as that of Gd(**8**).[41] Obviously, the long pendant arm in Gd(**3**) slows molecular rotation in this complex resulting in a higher relaxivity. The inner- and outer sphere

contribution to the r_{1p} relaxivity of Gd(**3**) and Gd(**6**) could also be estimated from the fitting of the NMRD profile (Figure 1). At 25°C and 20 MHz, the inner-sphere relaxivity (r_{1p}^{is}) of Gd(**3**) (4.0 $m_M^{-1}s^{-1}$) is almost twice as high as that of Gd(**6**) (2.4 $m_M^{-1}s^{-1}$) due to its slower tumbling rate. On the other hand, as expected, the contribution of the outer-sphere water molecules to the overall relaxivity (r_{1p}^{os}) is comparable (2.5 $m_M^{-1}s^{-1}$) for both complexes. This value is also in good agreement with the r_{1p} value of Gd(**7**) (r_{1p}=2.5 $m_M^{-1}s^{-1}$, 25°C, 20 MHz), a complex whose water proton longitudinal relaxation rate is dominated by the outer-sphere relaxation due to the very slow exchange between the inner-sphere water molecule and the bulk water.[49]

MRI of cells

Cellular uptake of Gd(**3**) (or Gd(**6**) as control) under hypoxic *versus* normoxic conditions was first examined using 9L rat glioma cells as an *in vitro* model. This cell line has been extensively used in the past as a hypoxia model in radiosensitivity studies under low oxygen conditions.[52–54] In our experiments, hypoxia was induced in 9L cells by exposing a plate of cells to nitrogen gas at a rate of 1L/min for two hours at room temperature prior to the addition of the complex. After this induction phase, the cells were incubated with either 5 m_M Gd(**3**) or Gd(**6**) for two hours under a continuous flow of nitrogen gas. The control consisted of the same cells exposed to the same concentration of each agent but using a constant flow of air rather than nitrogen. In addition, a negative control was prepared in which cells were incubated with PBS buffer alone (no gadolinium). After the incubation period, the samples were washed with PBS, detached from the culture plates using trypsin, pelleted into centrifuge tubes, and imaged immediately at 4.7T. T_1-weighted images and T_1 maps for three samples 1) negative control (C), 2) normoxic incubation (N) and 3) hypoxic incubation (H) of each complex are shown in Figure 2.

If the nitroimidazole moiety in Gd(**3**) undergoes reduction and is trapped in hypoxic cells, then the accumulation of Gd(**3**) should result in brighter proton images as a result of the shortening of T_1 of the bulk water by the intracellular agent. As seen from the T_1-weighted images in Figure 2, the hypoxic sample (H) has higher signal intensity when compared to the other two samples, whereas the normoxic and negative control samples are indistinguishable. The T_1 maps also show that cells incubated with Gd(**3**) under normoxic conditions have a somewhat shorter T_1 than the negative control cells. The average T_1 values for the negative controls, the normoxic incubation samples and the hypoxic incubation samples were 1.6±0.2 s, 1.4±0.1 s, and 0.8±0.1 s, respectively. This illustrates that Gd(**3**) enters cells by passive diffusion in both cell samples (normoxia and hypoxia) and a small amount of complex likely gets trapped even in normoxic cells. Nevertheless, the hypoxic cell pellet displays the shortest T_1 of the three samples. Converting the values to relaxation rates (0.64±0.09, 0.74±0.14 and 1.31±0.33 s^{-1}, respectively) highlights the differences in R_{1p}. Subtraction of the R_1 value for the negative control (cells only, no Gd(**3**)), yields R_{1p} values of 0.10 and 0.67 s^{-1} for the samples incubated with Gd(**3**) under normoxic and hypoxic conditions, respectively. Thus, the hypoxic cells accumulate ~2-fold more Gd(**3**) compared to normoxic cells. In comparison, the distribution of T1 values found for normoxic and hypoxic cells incubated with Gd(**6**) are significantly different ($p<0.05$) from the negative control but not from each other. The R_{1p} values of for the samples are 0.45 and 0.56 s^{-1} under normoxic and hypoxic conditions, respectively. While the two complexes (Gd(**3**) and Gd(**6**)) appear to accumulate to about the same extent in hypoxic cells as the nitroimidazole derivative, only Gd(**3**) shows hypoxia selectivity. The higher uptake of Gd(**6**) indicates that its uptake and retention is mediated by an oxygen-independent factor other than just passive diffusion. The higher uptake of Gd(**6**) may reflect its lower molecular weight and/or higher lipophilicity. Whatever the exact reasons for the

nonselective uptake of Gd(**6**), the important fact is that this complex does not show hypoxia selectivity, while Gd(**3**) exhibits selective hypoxia-mediated retention.

Conclusion

DO3A-monoamide conjugate of 2-nitroimidazole (ligand **3**) was synthesized and its complexes with Gd^{III} and other lanthanide ions characterized. As expected, the protonation constants of this ligand and stability of the resulting lanthanide ion complexes are quite comparable to published values for similar compounds. The ligand has a total of five protonation steps in the pH range of 2–12; two of these are assigned to the protonation of two macrocyclic nitrogen atoms. The stability of the Ln(**3**) complexes ranges from 19.24 to 21.51 for Ce^{III} to Lu^{III}, about four orders of magnitude lower than that of the corresponding $Ln(DOTA)^{-}$ complexes. This is in accordance with the lower total basicity of **3** compared to DOTA. The r_{1p} relaxivity, residence time of the metal bound water molecule (τ_M) and rotational correlation time (τ_R) of Gd(**3**) was determined by relaxivity measurements, variable temperature ^{17}O NMR and proton nuclear magnetic relaxation dispersion (NMRD) studies and the data ($r_{1p} = m_M^{-1}s^{-1}$, 6.38 ($\tau_M = 0.71$ μs, $\tau_R = 141$ ps) are in agreement with those obtained for other Gd^{III} complexes of similar size. *In vitro* MRI experiments with hypoxic 9L rat glioma cells revealed that Gd(**3**) is selectively trapped in hypoxic cells as evidenced by a nearly 2-fold contrast enhancement in the images of cells compared to normoxic cells. This suggests that this nitroimidazole conjugate may be suitable for assessment of hypoxia *in vivo*. Preliminary MR imaging of tumor bearing rats indicates that Gd(**3**) indeed accumulates largely in hypoxic tissues.[55]

Experimental Section

Abbreviations

MRI - magnetic resonance imaging; PET - positron emission tomography; SPECT - single photon emission computed tomography; L - ligand; DOTA - 1,4,7,10-tetraazacyclododecane-1,4,7,10-tetraacetic acid; DO3A - 1,4,7,10-tetraazacyclododecane-1,4,7-triacetic acid; PCTA - pyclen triacetic acid; NMRD- nuclear magnetic resonance dispersion; ROI - region of interest.

General

Details of all synthetic procedures, characterization of all intermediates, preparation of the Gd^{III} complexes, pH potentiometric titrations of ligands and complexes are reported in ESI.

Relaxivity and NMRD measurements

T_1 values were recorded at 20 MHz (0.47 T), 25°C and 37°C using a Stelar Spinmaster spectrometer (Stelar, Italy) and a Maran Ultra relaxometer (Oxford Instruments, United Kingdom) at 23 MHz and 37°C. Longitudinal relaxation times were measured using the inversion-recovery pulse sequence (180° – τ – 90°). The T_1 relaxivities were determined by the linear regression analysis of the water proton relaxation rates in solutions ranging in concentration from 0.2 to 21 mM, 50 mM HEPES buffer, in triplicate. The NMRD profiles were recorded on 1 mM samples over a continuum of magnetic field strengths from 0.00024 to 0.47 T (corresponding to 0.01 – 20 MHz proton Larmor Frequency) at 25°C using a Stelar field-cycling relaxometer under computer control with an absolute uncertainty of 1%. Relaxation data covering the range 0.47 T (20 MHz) to 1.7 T (70 MHz) were collected using a Stelar Spinmaster spectrometer operating at variable fields.

Variable temperature ^{17}O NMR measurements

^{17}O NMR linewidth data were collected using a Bruker DRX 600 NMR (14.1 T) spectrometer equipped with a 5 mm probe and a Bruker VT-1000 thermocontroller. NMR data were acquired by using a spectral width of 10,000 Hz, a 90° pulse (7 μs), an acquisition time of 10 ms, 1000 scans and no sample spinning. Water enriched in ^{17}O to 2.6% (Yeda, Israel) was used. The observed transverse relaxation rates (R^{O}_{2obs}) were calculated from the signal width at half-height ($\Delta\nu_{1/2}$): $R^{O}_{2obs} = \pi\ \Delta\nu_{1/2}$ The paramagnetic contribution to the water ^{17}O transverse relaxation rate (R^{O}_{2p}) were calculated from the R^{O}_{2obs} values according to the following equation: $R^{O}_{2p} = R^{O}_{2obs} - R^{O}_{2d}$ where R^{O}_{2d} is the water ^{17}O transverse relaxation rate in the absence of a GdL complex. The concentrations of Gd(**3**) and Gd(**6**) used for ^{17}O NMR measurements were 21 and 19 mM, respectively.

In vitro cell experiments

Rat 9L-glioma cells were grown to confluence in Dulbecco Modified Eagle Medium (DMEM) supplemented with 10% fetal bovine serum, 1% L-glutamine and 1% penicillin/streptomycin. The growth medium was replaced with 8 mL of un-supplemented DMEM prior to the uptake experiment. One plate (100 mm i.d.) of cells was made hypoxic by exposing it to nitrogen gas (1 L/min) in an enclosed chamber for two hours at room temperature while two other plates were exposed to room air. 1 mL of phosphate buffer saline (PBS) was then added to one of the two normoxic samples (as negative control), and 1 mL of 45 mM Gd(**3**) to the remaining two samples (one normoxic and one hypoxic) yielding a final concentration of 5 mM. The same procedure was followed to prepare three other samples (control, normoxic and hypoxic) for assessing cell uptake of Gd(**6**). These samples were incubated for two hours at room temperature (negative control and reference samples in air, hypoxic sample in nitrogen at 1 L/min), rinsed three times with PBS, trypsinized to release the cells, and centrifuged in 15 mL tubes at 2500 rpm for 5 min. Excess buffer was removed from the pellets, and the samples were transferred to 0.2 mL tubes for a final centrifugation at 14,500 rpm for 5 min.

MRI imaging of cells

The three sample tubes were positioned in a 2 cm volume coil and imaged at 4.7 T. Images were collected using a T_E of 12 ms and ten different T_R values ranging from (0.1 s – 6 s). A T_1 map was computed on a voxel-by-voxel basis from a least-squares fitting of the exponential relaxation curves using Varian software (VNMR 6.1C). Using software written in MATLAB, a region of interest (ROI) analysis was performed to extract voxel T_1 values for each pellet for statistical comparisons. The voxel T_1 data were imported into Origin 6.1 (OriginLab, Northampton, MA, USA) for student t-test analyses.

Supplementary Material

Refer to Web version on PubMed Central for supplementary material.

Acknowledgments

This work was supported in part by grants from the National Institutes of Health (CA-126608, RR-02584, CA-84697, and CA-115531) (ADS), the Robert A. Welch Foundation (AT-584) (ADS), the Hungarian Scientific Research Found (OTKA K84291 (GT), OTKA PD-83253 (KFK)); the TÁMOP 4.2.1./B-09/1/KONV-2010-0007 and TÁMOP-4.2.2./B-10/1-2010-0024 projects implemented through the New Hungary Development Plan, co-financed by the European Social Fund and the European Regional Development Fund and by the János Bolyai Research Scholarship (GT) of the Hungarian Academy of Sciences. This work has been carried out in the frame of the COST CM1006 “EUFEN: European F-Element Network” and COST TD1004 “Theragnostics Imaging and Therapy: An Action to Develop Novel Nanosized Systems for Imaging-Guided Drug Delivery” Actions.

References

1. Wouters A, Pauwels B, F. Lardon JB, Vermorken JB. Oncologist. 2007; 12:690–712. [PubMed: 17602059]
2. Tatum JL, Kelloff GJ, Gillies RJ, Arbeit JM, Brown JM, Chao KSC, Chapman JD, Eckelman WC, Fyles AW, Giaccia AJ, Hill RP, Koch CJ, Krishna MC, Krohn KA, Lewis JS, Mason RP, Melillo G, Padhani AR, Powis G, Rajendran JG, Reba R, Robinson SP, Semenza GL, Swartz HM, Vaupel P, Yang D, Croft B, Hoffman J, Liu G, Stone H, Sullivan D. Int. J. Radiat. Biol. 2006; 82:699–757. [PubMed: 17118889]
3. Nakamura S. Pharm. Bull. 1955; 3:379–383. [PubMed: 13289298]
4. Sheldon PW, Foster JL, Fowler JF. Br. J. Cancer. 1974; 30:560–565. [PubMed: 4451633]
5. Brown JM. Radiat. Res. 1975; 64:633–647. [PubMed: 1197663]
6. Edwards DI. J. Antimicrob. Chemother. 1993; 31:9–20. [PubMed: 8444678]
7. Knox RJ, Knight RC, Edwards DI. Br. J. Cancer. 1981; 44:741–745. [PubMed: 7032569]
8. Adams GE, Clarke ED, Flockhart IR, Jacobs RS, Sehmi DS, Stratford IJ, Wardman P, Watts ME, Parrick J, Wallace RG, Smithen CE. Int. J. Radiat. Biol. Relat. Stud. Phys. Chem. Med. 1979; 35:133–150. [PubMed: 312783]
9. Rasey JS, Krohn KA, Freauff S. Radiat. Res. 1982; 91:542–554. [PubMed: 7122830]
10. Grierson JR, Link JM, Mathis CA, Rasey JS, Krohn KA. J. Nucl. Med. 1989; 30:343–350. [PubMed: 2738663]
11. Ballinger JR, Kee JW, Rauth AM. J. Nucl. Med. 1996; 37:1023–1031. [PubMed: 8683295]
12. Das T, Chakraborty S, Banerjee S, Mukherjee A, Samuel G, Sarma HD, Nair CKK, Kagiya VT, Venkatesh M. Bioorg. Med. Chem. 2004; 12:6077–6084. [PubMed: 15519153]
13. Norman TJ, Smith FC, Parker D, Harrison A, Royle L, Walker CA. Supramol. Chem. 1995; 4:305–308.
14. Hoigebazar L, Jeong JM, Hong MK, Kim YJ, Lee JY, Shetty, Y.-S. Lee D, Lee, J.-K. Chung DS, Lee MC. Bioorg. Med. Chem. 2011; 19:2176–2181. [PubMed: 21419635]
15. Maxwell RJ, Workman P, Griffiths JR. Int. J. Radiat. Oncol., Biol., Phys. 1989; 16:925–929. [PubMed: 2703398]
16. Aboagye EO, Lewis AD, Johnson A, Workman P, Tracy M, Huxham IM. Br. J. Cancer. 1995; 72:312–318. [PubMed: 7640211]
17. Seddon BM, Payne GS, Simmons L, Ruddle R, Grimshaw R, Tan S, Turner A, Raynaud F, Halbert G, Leach MO, Judson I, Workman P. Clin. Cancer Res. 2003; 9:5101–5112. [PubMed: 14613987]
18. Aime S, Crich SG, Gianolio E, Giovenzana GB, Tei L, Terreno E. Coord. Chem. Rev. 2006; 250:1562–1579.
19. Hylton N. J. Clin. Oncol. 2006; 24:3293–3298. [PubMed: 16829653]
20. De Leon-Rodriguez LM, Kovacs Z. Bioconjugate Chem. 2008; 19:391–402.
21. Brown JM, Workman P. Radiat. Res. 1980; 82:171–190. [PubMed: 7367588]
22. Andre JP, Geraldes CFGC, Martins JA, Merbach AE, Prata MIM, Santos AC, de Lima JJP, Toth E. Chem.--Eur. J. . 2004; 10:5804–5816. [PubMed: 15472943]
23. Hay MP, Wilson WR, Moselen JW, Palmer BD, Denny WA. J. Med. Chem. 1994; 37:381–391. [PubMed: 8308864]
24. Dourtoglou V, Gross B, Lambropoulou V, Zioudrou C. Synthesis. 1984:572–574.
25. Knorr R, Trzeciak A, Bannwarth W, Gillessen D. Tetrahedron Lett. 1989; 30:1927–1930.
26. Sherry AD, Brown RD III, Geraldes CFGC, Koenig SH, Kuan KT, Spiller M. Inorg. Chem. 1989; 28:620–622.
27. Aime S, Anelli PL, Botta M, Fedeli F, Grandi M, Paoli P, Uggeri F. Inorg. Chem. 1992; 31:2422–3428.
28. Aime S, Barge A, Bruce JI, Botta M, Howard JAK, Moloney JM, Parker D, de Sousa AS, Woods M. J. Am. Chem. Soc. 1999; 121:5762–5771.
29. Lloyd GO, Luckay RC. Acta Crystallogr., Sect. E: Struct. Rep. Online. 2005; E61:o3405–o3407.

30. Kubicek V, Havlickova J, Kotek J, Tircso G, Hermann P, Toth E, Lukes I. Inorg. Chem. 2010; 49:10960–10969. [PubMed: 21047078]
31. Martell, AE.; Smith, RM.; Motekaitis, RJ. Critically Selected Stability Constants of Metal Complexes Database. 8 ed.. College Station, TX: Texas A&M University; 2004.
32. Chaves S, Delgado R, Frausto da Silva JJR. Talanta. 1992; 39:249–254. [PubMed: 18965370]
33. Burai L, Fabian I, Kiraly R, Szilagyi E, Brucher E. J. Chem. Soc., Dalton Trans. 1998:243–248.
34. Keire DA, Kobayashi M. Bioconjugate Chem. 1999; 10:454–463.
35. Pasha A, Tircso G, Benyo ET, Brucher E, Sherry AD. Eur. J. Inorg. Chem. 2007:4340–4349. [PubMed: 19802361]
36. Kumar K, Chang CA, Francesconi LC, Dischino DD, Malley MF, Gougoutas JZ, Tweedle MF. Inorg. Chem. 1994; 33:3567–3575.
37. Cacheris WP, Nickle SK, Sherry AD. Inorg. Chem. 1987; 26:958–960.
38. Caravan P, Ellison JJ, McMurry TJ, Lauffer RB. Chem. Rev. 1999; 99:2293–2352. [PubMed: 11749483]
39. Lauffer RB. Chem. Rev. 1987; 87:901–927.
40. Bruce, JI.; Lowe, MP.; Parker, D. The Chemistry of Contrast Agents in Medical Magnetic Resonance Imaging. Merbach, AE.; Toth, E., editors. Chichester: John Wiley & Sons; 2001. p. 437-460.
41. GeninattiCrich SG, Cabella C, Barge A, Belfiore S, Ghirelli C, Lattuada L, Lanzardo S, Mortillaro A, Tei L, Visigalli M, Forni G, Aime S. J. Med. Chem. 2006; 49:4926–4936. [PubMed: 16884304]
42. Aime S, Botta M, Crich SG, Giovenzana G, Pagliarin R, Sisti M, Terreno E. Magn. Reson. Chem. 1998; 36:S200–S208.
43. Aime S, Botta M, Fasano M, Paoletti S, Terreno E. Chem.-Eur. J. 1997; 3:1499–1504.
44. Powell DH, Ni Dhubhghaill OM, Pubanz D, Helm L, Lebedev YS, Schlaepfer W, Merbach AE. J. Am. Chem. Soc. 1996; 118:9333–9346.
45. Swift TJ, Connick RE. J. Chem. Phys. 1962; 37:307–320.
46. Viswanathan S, Kovacs Z, Green KN, Ratnakar SJ, Sherry AD. Chem. Rev. 2010; 110:2960–3018. [PubMed: 20397688]
47. Banci, L.; Bertini, I.; Luchinat, C. Nuclear and Electronic Relaxation. Weinheim: VCH; 1991.
48. Korb JP, Ahadi M, Zientara GP, Freed JH. J. Chem. Phys. 1987; 86:1125–1130.
49. Aime S, Barge A, Botta M, Parker D, De Sousa AS. J. Am. Chem. Soc. 1997; 119:4767–4768.
50. Toth E, Connac F, Helm L, Adzamli K, Merbach AE. Eur. J. Inorg. Chem. 1998:2017–2021.
51. Bertini C, Luchinat I. Coord. Chem. Rev. 1996; 150:1–292.
52. Jounaidi Y, Waxman DJ. Cancer. Res. 2000; 60:3761–3769. [PubMed: 10919648]
53. Kirkpatrick JP, Cardenas-Navia LI, Dewhirst MW. Int. J. Radiat. Oncol. Biol. Phys. 2004; 59:822–833. [PubMed: 15183486]
54. Moriyama EH, Jarvi M, Niedre M, Mocanu JD, Moriyama Y, Li B, Lilge L, Wilson BC. Proc. SPIE-Int. Soc. Opt. Eng. 2007; 6449:64490F/1–64490F/8.
55. Kodibagkar, VD.; Gulaka, PK.; Rojas-Quijano, F.; Kovacs, Z.; Mason, RP.; Sherry, AD. Proc. Internat. Soc. Magn. Reson. Med. Montreal, Canada: 2011. p. 1672

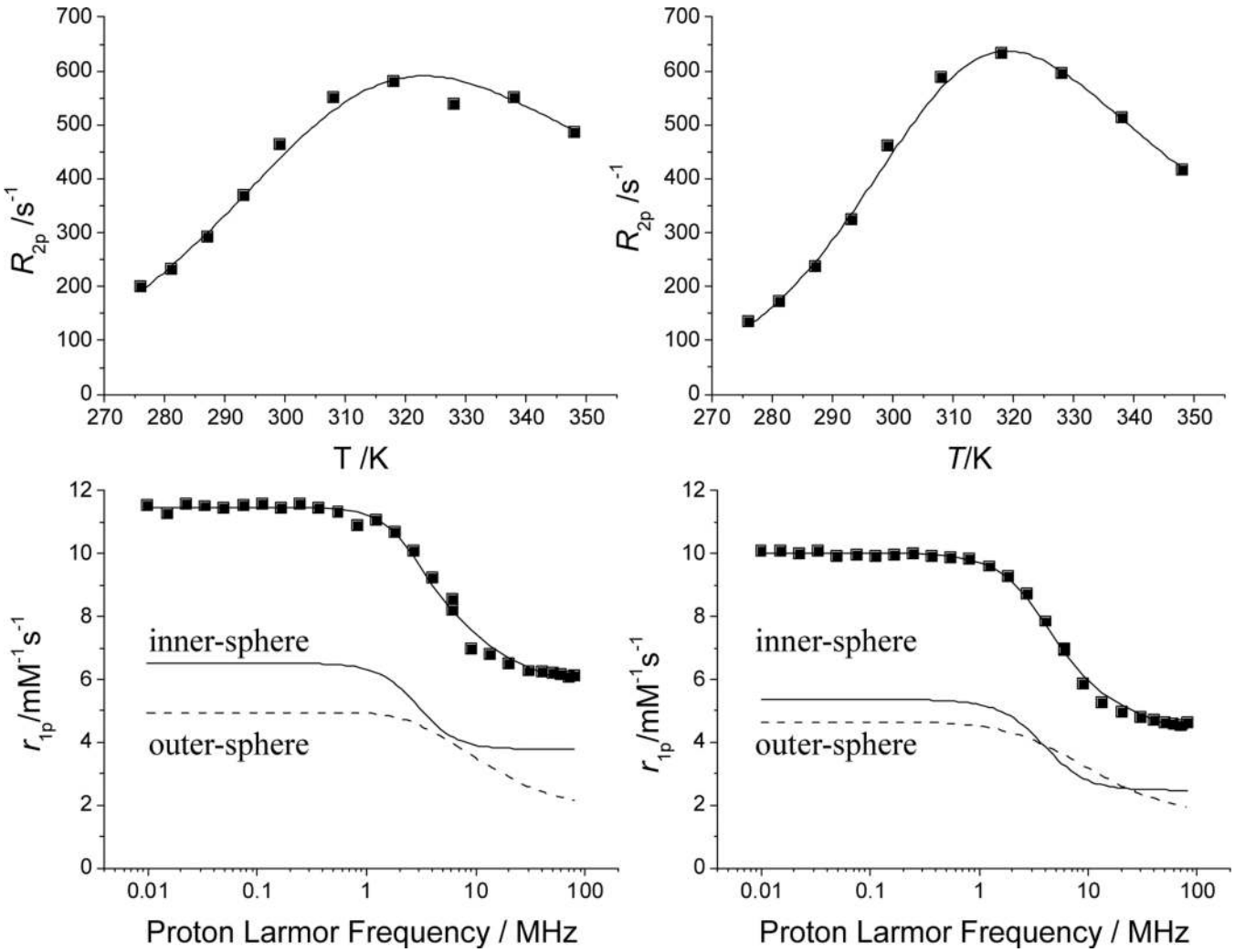

Figure 1.

(Top row) Temperature dependence of the transverse water ^{17}O NMR relaxation rates at 14.1T and pH=7 for 21 mM and 19 mM solutions of Gd(**3**) (left) and Gd(**6**) (right), respectively. (Bottom row) NMRD profiles of the 1 mM solutions of Gd(**3**) (left) and Gd(**6**) (right) at pH=7. The solid and dashed curves in the lower part represent the inner- and outer-sphere contributions to the overall relaxivity, respectively.

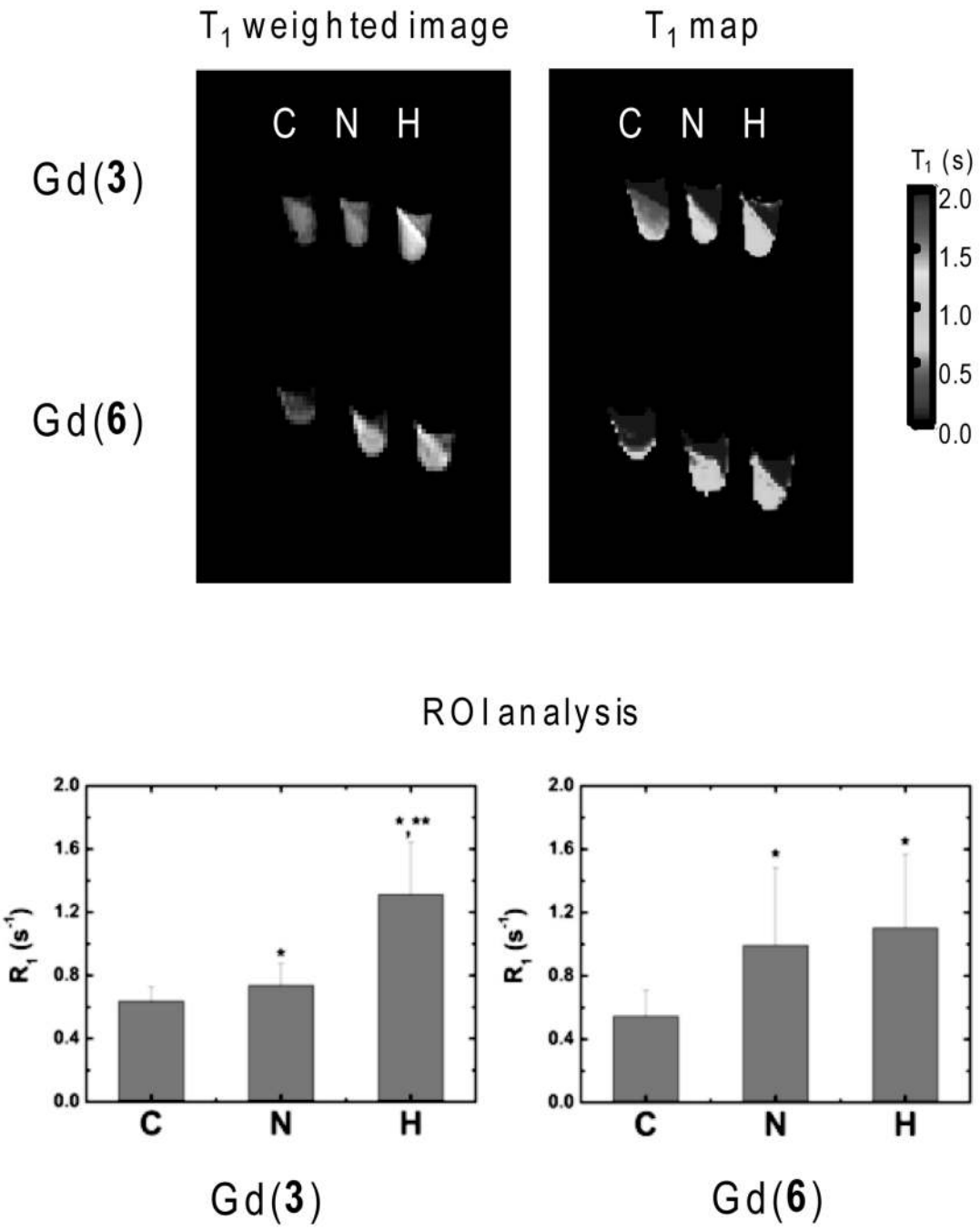

Figure 2.

In vitro MR imaging of 9L rat glioma cells after exposure to either Gd(**3**) or Gd(**6**) (top). T_1-weighted images (T_R = 300 msec; T_E = 10 msec) and T_1 maps of negative control (C), normoxic (N) and hypoxic (H) cells. Relaxation rates (R_1) for the packed cell layers (bottom) (* = p <0.05 compared to negative control (C); ** = p<0.05 compared to normoxic sample (N)). Color version of Figure 2 is included in the Electronic Supporting Information.

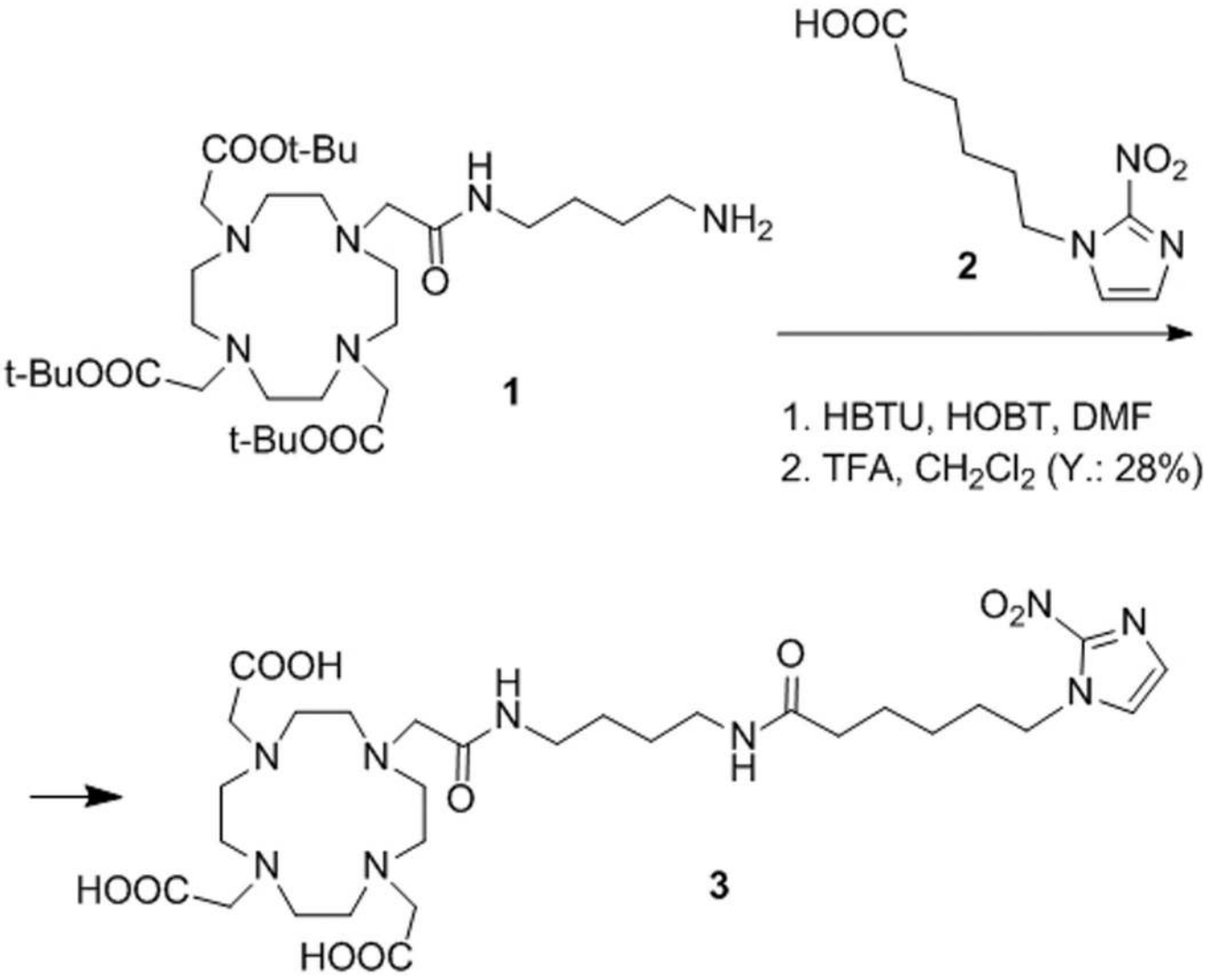

Scheme 1.
Synthetic route to ligand **3** (Y.: 28%).

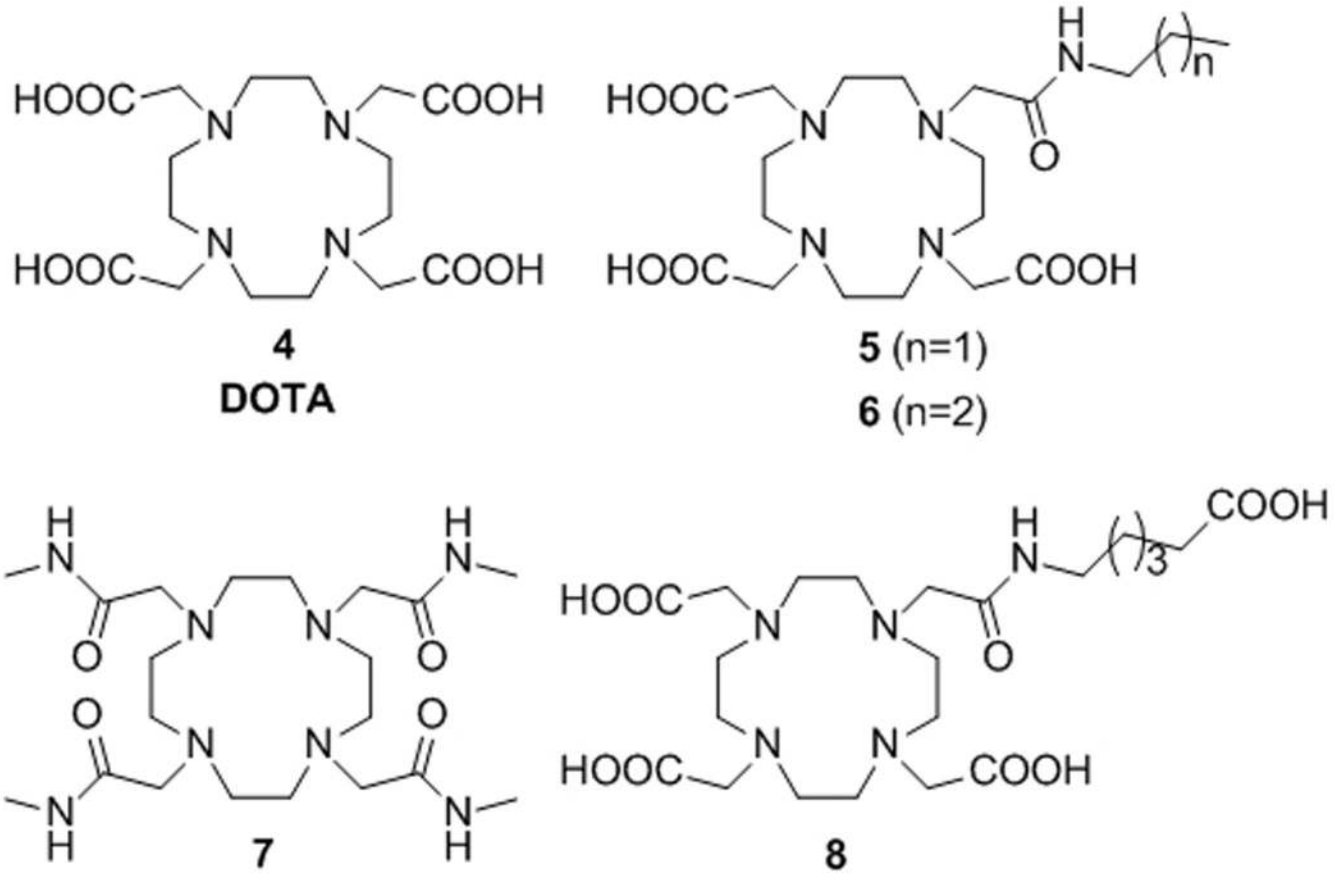

Chart 1.
The structures of DOTA (**4**), a DOTA-tetramethylamide (**7**) and some DO3A-monoamide derivatives (**5, 6** and **8**) discussed in this work.

Table 1

Protonation constants[a] of **3** and some ligands of similar structure, 1 M KCl, 25 °C.

log *K*	**3**[b]	**4**	**5**[e]	**6**[b]	**7**[h]
log K_1^H	9.78(2)	12.09[c]; 12.6[d]	9.6	10.17(1), 12.22[f], 10.73[g]	9.56
log K_2^H	9.05(3)	9.67[c]; 9.70[d]	9.2	9.02(1), 8.90[f], 9.05[g]	5.95
log K_3^H	4.53(4)	4.55[c]; 4.50[d]	4.4	4.41(1), 4.34[f], 4.53[g]	–
log K_4^H	3.17(5)	4.09[c]; 4.14[d]	1.7	2.94(1), 2.49[f], 3.32[g]	–
log K_5^H	2.19(6)	2.32[d]	–	1.99(1), 1.47[f], 2.25[g]	–
log β_4	26.53	30.40[c]; 30.94[d]	24.9	26.54, 27.94[f], 27.63[g]	15.51[i]

[a] Standard deviations shown in parentheses.

[b] This work, in 1.0 M KCl and at 25 °C.

[c] In 0.1 M KCl.[32]

[d] In 1.0 M Me_4NCl.[33]

[e] In 0.1 M NaCl.[26]

[f] In 0.1 M Me_4NCl.[30]

[g] The ionic strength was not controlled (25 °C).[34]

[h] In 0.1 M KCl.[35]

[i] The value refers to log β_2, since this ligand has only two protonation constants.

Table 2

Thermodynamic stability constants and protonation constants of lanthanide complexes of ligands **3–7**, 25°C.

Ln^{III}	eq.	$_3$[a]	$_4$[c]	$_5$[f]	$_6$[a]	$_7$[h]
Ce^{III}	log $K_{Ln•L}$	19.2(0.1)	23.39, 22.86[d]	–	19.26(4)	12.68
	log $K_{LnL•H}$[b]	–	2.5[d]	–	2.65(5)	–
Gd^{III}	log $K_{Ln•L}$	20.93(9)	24.67, 25.3[e]	20.1	21.29(1)	13.54
	log $K_{LnL•H}$	2.93(4)	2.3	–	2.57(1)	–
Lu^{III}	log $K_{Ln•L}$	21.51(9)	25.41, 25.0[e]	–	21.83(3)[g]	13.91
	log $K_{LnL•H}$	2.44(9)	–	–	2.33(4)	–

[a] This work in 1.0 M KCl.

[b] log $K_{LnL•H} = [LnHL]/[LnL][H^+]$.

[c] Ref.[36,37].

[d] Data correspond to the La^{III} complex.

[e] Ref.[36,37].

[f] In 0.1 M NaCl Ref.[26]

[g] Data correspond to the Yb^{III} complex.

[h] In 1.0 M KCl.[35]

Table 3

Relaxation parameters calculated from the simultaneous fitting of the temperature dependence of the water ^{17}O transverse relaxation rate and the NMRD profiles of Gd(**3**) and Gd(**6**).

	Gd(3)	Gd(6)	Gd(8)[a]
r_{1p}^{298} [$mM^{-1}s^{-1}$]	6.38 ± 0.04	5.05 ± 0.02	5.0
q	1	1	1
Δ^2 [$s^{-2} \times 10^{19}$]	1.9 ± 0.1[b]	1.0 ± 0.1[b]	1.4
τ_v^{298} [ps]	58 ± 7[b]	34 ± 4[b]	40
τ_R^{298} [ps]	141 ± 3[b]	86 ± 2[b]	70
τ_M^{298} [ps]	0.71 ± 0.09[c]	0.66 ± 0.05[c]	1.3
ΔH_M [$kJ \times mol^{-1}$]	28 ± 4[c]	40 ± 3[c]	19
ΔH_V [$kJ \times mol^{-1}$]	25 ± 10[c]	28 ± 10[c]	40

[a] Ref.[41].

[b] Best-fit parameters obtained from the analysis of the NMRD profile using the standard value for the average distance between the metal and protons of the inner-sphere water molecule (a = 3.8 Å), and 2.24×10^{-5} cm^2 s^{-1} for the self-diffusion coefficient of water (D).[43,50]

[c] Best-fit parameters obtained from the analysis of the temperature dependence of ^{17}O NMR transverse relaxation rate in 21 and 19 mM solutions of Gd(**3**) and Gd(**6**), respectively, assuming a Gd^{3+} – ^{17}O scalar coupling constant of -3.8×10^6 rad s^{-1} and a Gd^{III} – ^{17}O distance of 2.5 Å.[44,51]